ARTICLES
https://doi.org/10.1038/s41557-018-0195-4
nature chemistry

Transition-metal-bridged bimetallic clusters with multiple uranium–metal bonds

Genfeng Feng[1], Mingxing Zhang[1], Dong Shao[1], Xinyi Wang[1], Shuao Wang[2], Laurent Maron[3]* and Congqing Zhu[1]*

Heterometallic clusters are important in catalysis and small-molecule activation because of the multimetallic synergistic effects from different metals. However, multimetallic species that contain uranium–metal bonds remain very scarce due to the difficulties in their synthesis. Here we present a straightforward strategy to construct a series of heterometallic clusters with multiple uranium–metal bonds. These complexes were created by facile reactions of a uranium precursor with $Ni(COD)_2$ (COD, cyclooctadiene). The multimetallic clusters' cores are supported by a heptadentate N_4P_3 scaffold. Theoretical investigations indicate the formation of uranium–nickel bonds in a U_2Ni_2 and a U_2Ni_3 species, but also show that they exhibit a uranium–uranium interaction; thus, the electronic configuration of uranium in these species is U(III)-5$f^2$6d^1. This study provides further understanding of the bonding between *f*-block elements and transition metals, which may allow the construction of *d*–*f* heterometallic clusters and the investigation of their potential applications.

Multimetallic molecules are of great interest because of their fascinating structures and multimetallic synergistic effects for catalysis and small molecule activation[1–7]. Both biological nitrogen fixation and industrial Haber–Bosch ammonia syntheses, for example, are thought to utilize multimetallic catalytic sites[8,9]. Meanwhile, the chemistry of uranium–metal bonds has also attracted many theoreticians and experimentalists[10–12], partly because uranium exhibits intriguing properties in both catalysis and energy[13–22]. Recently, Mazzanti and co-workers reported nitrogen functionalization by a multimetallic diuranium(III) species[20]. However, multimetallic diuranium species that contain uranium–metal bonds remain undeveloped due to the absence of an efficient synthetic strategy.

The first known complex to contain a uranium–metal bond was reported in 1987 by Sternal and Marks[23], but research on this chemistry was dormant for two decades and has only recently begun to be revived[24–38]. Heterobidentate ligands are typically used to stabilize transition metal–metal bond species[39–42], and are also effective for the synthesis of complexes with supported uranium–metal bonds. Two typical examples are the phosphinoamide ligand (**I** in Fig. 1a) with a rigid nitrogen–phosphorus scaffold[32] and the diphenylphosphine-substituted aryloxide ligand (**II** in Fig. 1a) with an oxygen–phosphorus scaffold[35,36]. These ligands are useful in the synthesis of heterobimetallic complexes with uranium–metal (Co, Ni, Pd, Pt and Rh) bonds. Significantly, Arnold and co-workers reported a novel synthetic route for a uranium–cobalt bond, which was generated by photolysis of an isocarbonyl species with a heptadentate N_4P_3 scaffold (**III** in Fig. 1a)[33]. These ligand scaffolds, however, support only one uranium–metal bond and the oxidation state of uranium in these species is +IV.

Here we report a straightforward strategy to construct a series of unprecedented multimetallic bridged clusters with four or six uranium–metal bonds by employing a new heptadentate N_4P_3 scaffold[43] with three rigid nitrogen–phosphorus units (**IV** in Fig. 1a). This study offers a new opportunity to investigate *d*–*f* heteromultimetallic clusters with multiple uranium–metal bonds for small-molecule activation and catalysis.

Results and discussion

Synthesis and structural characterization. Complex **1** (Fig. 1b), a trilithium salt, was easily prepared in a nearly quantitative yield by the reaction of $N[CH_2CH_2NHP^iPr_2]_3$ with three equivalents of *n*-BuLi in tetrahydrofuran (THF). The structure of this lithiated product was fully characterized by NMR spectroscopy (Supplementary Figs. 1–3), elemental analysis and X-ray crystallography. After reacting complex **1** with uranium tetrachloride (UCl_4) at room temperature (r.t.), complex **2** was isolated as a brown solid in a 59% yield after recrystallization from toluene at −30 °C. The ^{1}H NMR spectrum of complex **2** exhibits a broad range of peaks from +30 to −10 ppm and is consistent with the spectra of other tetravalent uranium complexes that contain tren-based ligands (Supplementary Fig. 4)[44]. The ^{31}P NMR resonance of complex **2** (739.71 ppm, Supplementary Fig. 5) strongly shifted downfield compared with that of complex **1** (70.98 ppm).

The molecular structure of complex **2** was determined by single-crystal X-ray diffraction. As shown in Fig. 2a, complex **2** crystallizes with a three-fold symmetry, which is consistent with the five resonances observed in its ^{1}H NMR spectrum in solution (Supplementary Fig. 4). The uranium in complex **2** is eight-coordinated to four nitrogen atoms, three phosphorus atoms and one chlorine atom. This coordination pattern is slightly different from that observed in the uranium complex that employs **III** as a ligand[33]. In general, the bond lengths of the U–N_{amido}, U–N_{amine} and U–P bonds in complex **2** are similar to those previously reported for uranium complexes with ligands **I**, **II** and **III**.

With complex **2** in hand, we attempted to synthesize multimetallic clusters with uranium–metal bonds. Treatment of **2** with one equivalent of $Ni(COD)_2$ (COD, cyclooctadiene) at room

[1]State Key Laboratory of Coordination Chemistry, Jiangsu Key Laboratory of Advanced Organic Materials, School of Chemistry and Chemical Engineering, Nanjing University, Nanjing, China. [2]State Key Laboratory of Radiation Medicine and Protection, School for Radiological and interdisciplinary Sciences (RAD-X) and Collaborative Innovation Center of Radiation Medicine of Jiangsu Higher Education Institutions, Soochow University, Suzhou, China. [3]LPCNO, CNRS & INSA, Université Paul Sabatier, Toulouse, France. *e-mail: laurent.maron@irsamc.ups-tlse.fr; zcq@nju.edu.cn

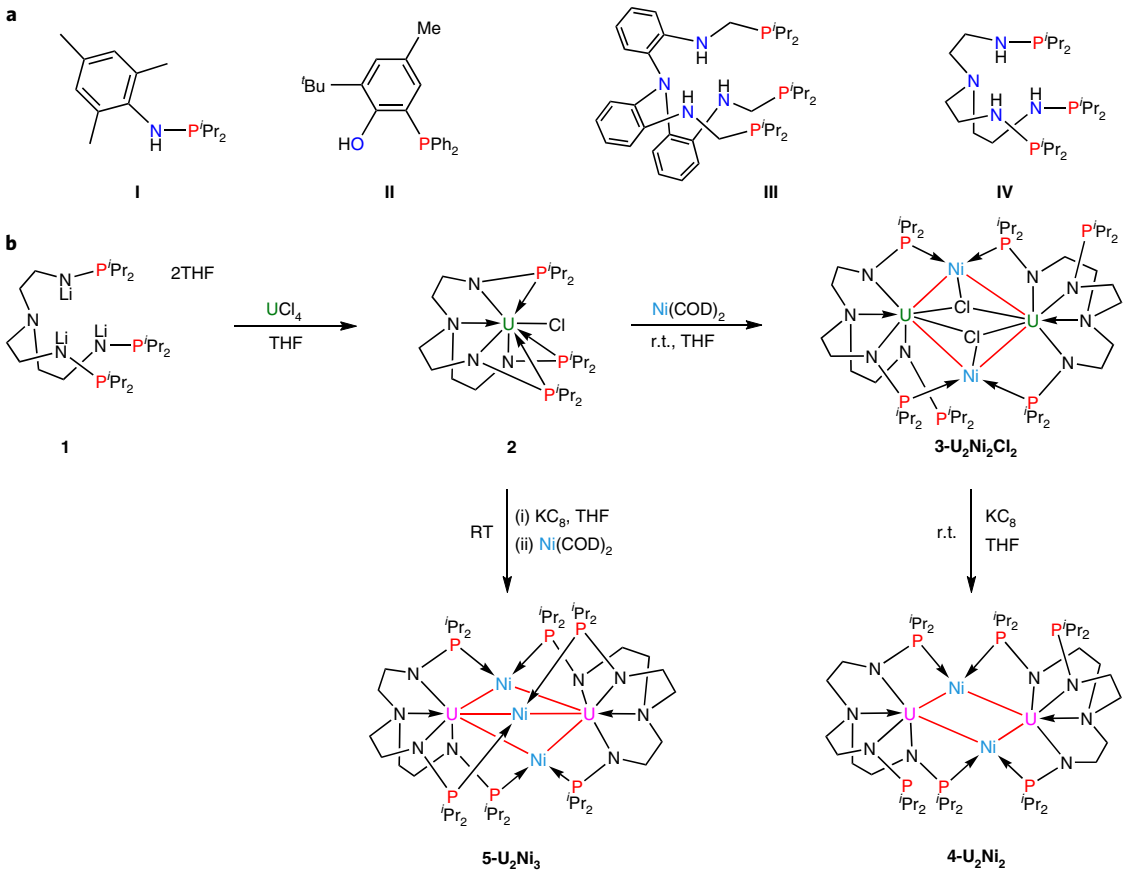

Fig. 1 | Synthesis of multimetallic bridged clusters. a, Representative ligands for supported uranium–metal bonds. **b**, Synthesis of the uranium precursor 2, the bimetallic bridged clusters **3-$U_2Ni_2Cl_2$** and **4-U_2Ni_2** and the trimetallic bridged cluster **5-U_2Ni_3**. The U–Ni bonds are shown in red. The green U atom indicates uranium(IV) and the pink colour denotes uranium(III).

temperature (r.t.) in THF afforded the dark-brown, crystalline complex **3-$U_2Ni_2Cl_2$** in a 46% yield (Fig. 1b). Using two or more equivalents of $Ni(COD)_2$ did not alter the reaction outcome. This complex is an unusual example of a metal-bridged bimetallic cluster with four uranium–metal bonds. The oxidation state of uranium in **3-$U_2Ni_2Cl_2$** is +IV. Therefore, we explored reduction strategies to synthesize a trivalent uranium–metal complex. A suspension of **3-$U_2Ni_2Cl_2$** and two equivalents of potassium graphite (KC_8) was stirred at r.t. overnight (Fig. 1b). Complex **4-U_2Ni_2** was isolated as black crystals in a 35% yield after recrystallization from toluene at −30 °C. The NMR characterization of these *d*–*f* heterometallic clusters, **3-$U_2Ni_2Cl_2$** and **4-U_2Ni_2**, was hindered by their poor solubility and, accordingly, elemental analysis and powder X-ray diffraction were used to verify the purities of the bulk samples (Supplementary Figs. 7 and 8).

The solid-state structures of **3-$U_2Ni_2Cl_2$** and **4-U_2Ni_2** were confirmed by X-ray crystallographic analyses (Fig. 2b,c), and the structures feature a heterometallic U–Ni_2–U core in which the two uranium atoms are bridged by two transition metals. The U1–Ni1 bond length (3.086(4) Å) in **3-$U_2Ni_2Cl_2$** is 10% longer than the sum of the covalent radii for the uranium–nickel single bond (2.80 Å) (ref. [45]). However, the U–Ni bond length is significantly shortened after the reduction. The four U–Ni bond lengths in **4-U_2Ni_2** have an average length of 2.844(9) Å (range of 2.688(9)–3.011(10) Å), which is close to the sum of the covalent single bond radii of uranium and nickel (2.80 Å). The bond lengths of U–N_{amido} (average of 2.278(2) Å in **3-$U_2Ni_2Cl_2$** and 2.281(6) Å in **4-U_2Ni_2**) and U–N_{amine} (2.681(2) Å in **3-$U_2Ni_2Cl_2$** and an average of 2.684(6) Å in **4-U_2Ni_2**) are consistent with those reported for uranium complexes with tren-based ligands[44]. These species feature transition-metal-bridged heterometallic clusters with multiple uranium–metal bonds.

Two uncoordinated phosphorus atoms (P3 and P6 in Fig. 2c) were observed in the solid state of **4-U_2Ni_2**. In principle, complex **4-U_2Ni_2** can react with $Ni(COD)_2$ to generate a trimetallic-bridged cluster, but our attempts in this regard were unsuccessful. To synthesize this species, a U(III) precursor was generated in situ by reducing complex **2** with KC_8 at r.t. (Fig. 1b). The filtrate was treated with 1.5 equivalents of $Ni(COD)_2$ in THF at r.t. overnight and then crystallized at −30 °C to yield the trimetallic-bridged diuranium cluster **5-U_2Ni_3** as black crystals in a 38% yield. The NMR characterization of **5-U_2Ni_3** was also hindered by its poor solubility and, accordingly, the purity of the bulk samples was confirmed by elemental analysis and powder X-ray diffraction (Supplementary Fig. 9). Complex **5-U_2Ni_3** is extremely sensitive to air and moisture, but is relatively stable in an inert atmosphere.

The molecular structure of complex **5-U_2Ni_3** was confirmed by single-crystal X-ray diffraction (Fig. 2d). The crystallographic analysis revealed that the molecule crystallizes in a monoclinic system with a *C*2/*c* space group. The average bond lengths of U–N_{amido} (2.242(10) Å) and U–N_{amine} (2.720(11) Å) are consistent with those reported for uranium complexes with tren-based ligands[44]. The most salient structural feature of **5-U_2Ni_3** is that the two uranium atoms are connected by three nickel(0) atoms. The uranium–nickel bond distances range from 2.775(3) to 2.967(2) Å, which are close to the bond distances of uranium–nickel observed in **4-U_2Ni_2** (range of 2.688(9)–3.011(10) Å). These U–Ni distances are slightly longer than those recently reported by Arnold and co-workers[35]. The high

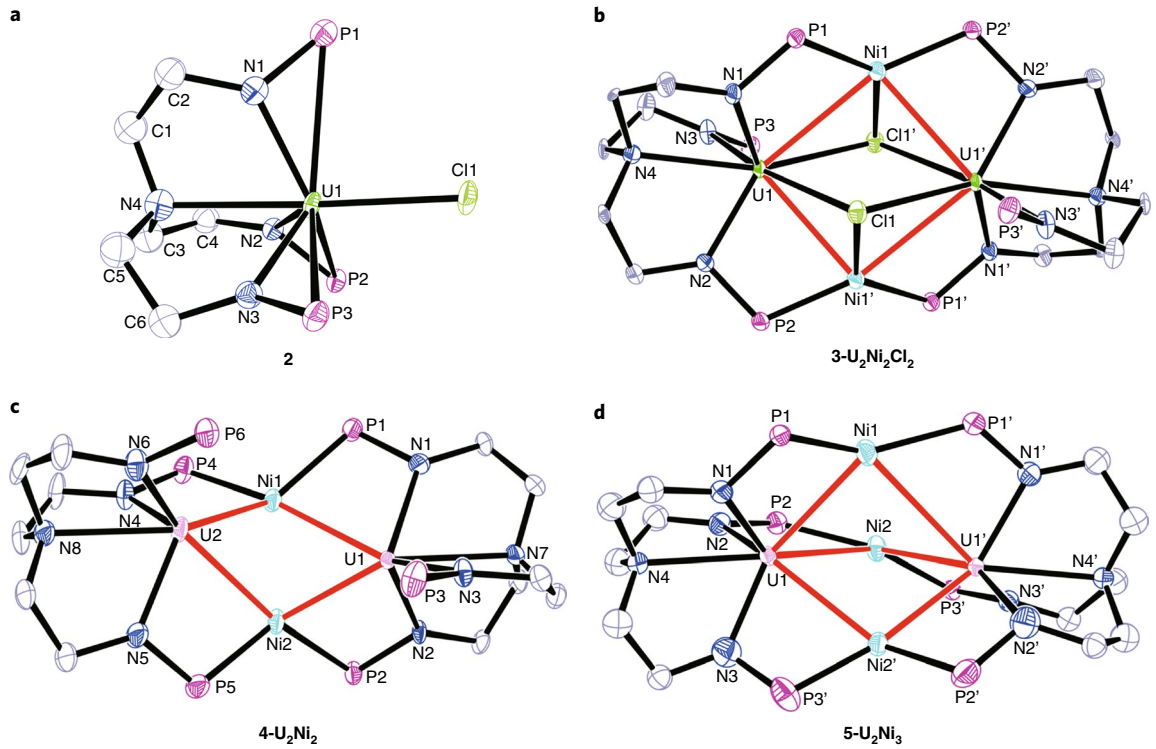

Fig. 2 | Molecular structures of 2, $3\text{-}U_2Ni_2Cl_2$, $4\text{-}U_2Ni_2$ and $5\text{-}U_2Ni_3$. a–d, Solid-state structures of **2** (**a**), $\mathbf{3\text{-}U_2Ni_2Cl_2}$ (**b**), $\mathbf{4\text{-}U_2Ni_2}$ (**c**) and $\mathbf{5\text{-}U_2Ni_3}$ (**d**) by X-ray crystallography with 50% probability ellipsoids. Solvent molecules, hydrogen atoms and isopropyl moieties in P^iPr_2 are omitted for clarity. The U–Ni bonds are shown in red. Uranium(IV), dark green; uranium(III), pink; nickel, cyan; phosphorus, violet; nitrogen, blue; chlorine, light green; carbon, grey.

number of uranium–nickel bonds observed in $\mathbf{5\text{-}U_2Ni_3}$ is noteworthy. We also tried to synthesize the corresponding bimetallic clusters with multiple U–Pt bonds by using $Pt(COD)_2$ or $Pt(PPh_3)_4$ as the precursor[35,46,47]. Unfortunately, no single crystals suitable for X-ray diffraction are obtained as yet. Nevertheless, $\mathbf{3\text{-}U_2Ni_2Cl_2}$, $\mathbf{4\text{-}U_2Ni_2}$ and $\mathbf{5\text{-}U_2Ni_3}$ represent rare examples of transition-metal-bridged clusters with multiple uranium–metal bonds.

Computational analysis. Density functional theory (DFT) calculations were used to elucidate the bonding in these multimetallic-bridged clusters. Geometry optimizations were carried out on $\mathbf{3\text{-}U_2Ni_2Cl_2}$ assuming an oxidation state of +IV for the uranium centres. The optimized geometry (B3PW91) is in good agreement with the experimental geometry (in particular, the optimized U–Cl and U–Ni distances are 2.9 Å and 3.2 Å, respectively, which agree with the experimental average values of 2.890(7) Å and 3.156(4) Å). Natural bonding orbital analysis was then used to analyse the bonding. As expected, the formation of two strongly polarized U-Cl bonds (92% Cl and 8% U) was observed, but, more interestingly, a donor–acceptor interaction between Ni and U was found (donation from a *d* orbital of Ni into a hybrid *d*/*f* orbital of U). This bonding situation is corroborated by the Wiberg bond indexes (WBIs). The two WBI values for U–Cl are 0.46 (for comparison, the U–N ones are 0.40), and two U–Ni WBI values of 0.20 were also found, which indicates the presence of a U–Ni interaction. A similar computational procedure was applied to $\mathbf{4\text{-}U_2Ni_2}$. The uranium in this complex initially appears to be U(III), and therefore a $5f^3$ configuration is expected. The geometry was first optimized using small-core (explicit treatment of the 5*f* electrons) relativistic core potentials in either a septet or a quintet spin state. In this calculation, unexpectedly, the quintet was found to be lower in energy by 6.4 kcal mol^{-1} (0.28 eV). This means that in all the geometry optimizations the nickel atoms were found to exhibit a low-spin d^8 configuration. Before applying multireference calculations to understand this intermediate spin state, the validity of the small-core DFT calculation was tested by fixing the *f* electron configuration using *f*-in-core relativistic core potentials. Using this procedure (computational details given in the Supplementary Information), a geometry optimization was carried out assuming the expected $5f^3$ configuration (that means, similar to the septet spin state as ferromagnetic coupling is enforced with the fixed $5f^3$ core configuration). Surprisingly, the optimized geometry did not match with the experimental geometry at all (the U–Ni distances are 3.5 Å, that is, 0.7 Å longer than the experimentally determined distance and the U–U bond length is 4.6 Å versus the experimental 4.248(1) Å. The coordinates of the optimized structure are given in the Supplementary Information). Then, the geometry was optimized using the $5f^2$ electronic configuration, and the optimized geometry agreed with the experimental geometry (the computed average U–Ni distance is 2.9 Å versus 2.844(9) Å experimentally and the U–U distance is 4.4 Å versus the experimental 4.248(1) Å). The molecular orbitals obtained from the small-core calculations indicate the formation of a U–U interaction in a four-centre bond (Fig. 3a). This bond is formed using a *s*/*d* hybrid orbital from each U. This hybrid orbital is built on a mixture of the 7*s* (coefficient of 0.262 in the molecular orbital expansion) and the $6dz^2$ (coefficient of +0.195 or −0.195, depending on the U centre, to yield a bonding interaction). The contribution from the Ni atoms to this highest occupied molecular orbital (HOMO) involves the 4*s* orbital (coefficient of 0.09 on each Ni), which indicates that the main contribution comes from uranium. This orbital is occupied by two electrons and results in a U(III)-$5f^26d^1$ configuration. The associated U–U WBI value is 0.20, which is the same as that for U–Ni in $\mathbf{3\text{-}U_2Ni_2Cl_2}$. The four U–Ni WBI values in $\mathbf{4\text{-}U_2Ni_2}$ are between 0.35 and 0.40, so that it is similar to the U–Cl interactions in $\mathbf{3\text{-}U_2Ni_2Cl_2}$. The same holds true when analysing the density from an *f*-in-core calculation.

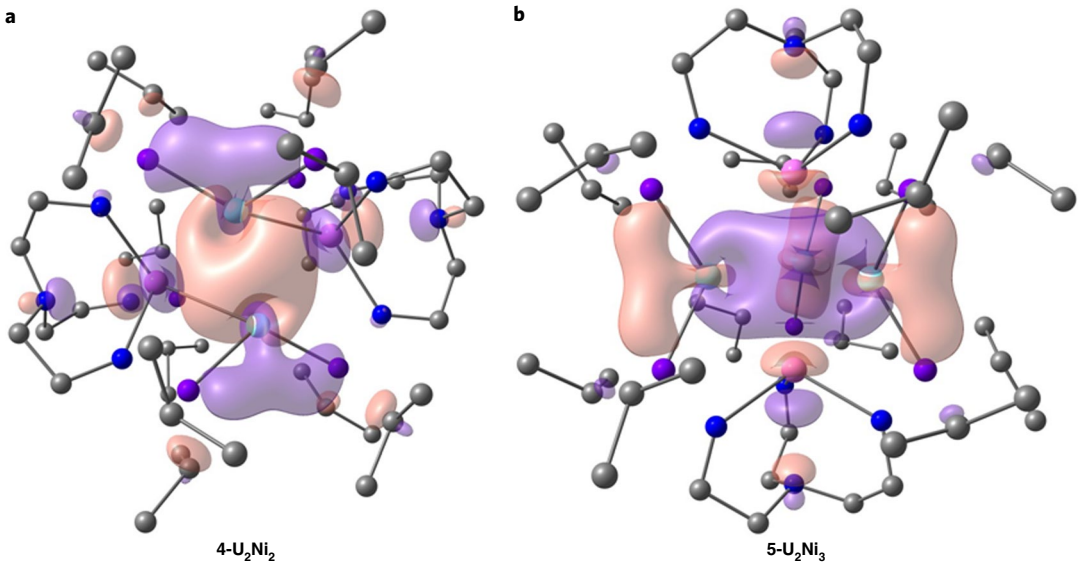

Fig. 3 | Highest doubly occupied molecular orbital of 4-U_2Ni_2 and 5-U_2Ni_3. a,**b**, The HOMO indicates a U–U interaction in a four-centre bond in **4-U_2Ni_2** (**a**) and a five-centre bond in **5-U_2Ni_3** (**b**). The colour code is the same as for Fig. 2.

DFT calculations were also used to elucidate the bonding in **5-U_2Ni_3**. Geometry optimizations were carried out without symmetry constraints with the same procedure applied as for **4-U_2Ni_2** and the optimized geometry was in good agreement with the experimental data. The calculated U–N bond distances were found to average 2.32 Å for the equatorial bonds and 2.70 Å for the apical bonds, which are in good agreement with the experimental bond lengths ($U–N_{amido}$ average of 2.242(10) Å and $U–N_{amine}$ of 2.720(11) Å). The optimized U–Ni distances were 3.05 Å on average, which was, due to the lack of crystal packing effects in the calculation, slightly longer than the value (average 2.894(3) Å) determined experimentally. The molecular orbitals, from the small-core calculation, revealed the formation of a U–U interaction in a five-centre bond (Fig. 3b). This bond uses a *s*/*d* hybrid orbital from each U, which is occupied by one electron to give a U(III)-$5f^26d^1$ configuration, and involves the empty p_y orbital on the three Ni centres. In the HOMO that is depicted, a hybrid *s*/*d* orbital on uranium is formed (0.383 from 7*s* and +0.274 or −0.274 from $6dz^2$, depending on the U centre) and each of the Ni interacts through an empty *p* orbital whose coefficients are 0.08 each (in fact, it is 0.08 on each p_y). The associated U–U WBI value is 0.19, which is consistent with the bonding interaction found in the HOMO of the system. For comparison, the U–N WBI values are 0.40 and the U–Ni WBI values are 0.27, which shows that the U–U interaction is not weak. Therefore, these multimetallic clusters, **4-U_2Ni_2** and **5-U_2Ni_3**, contain multiple U–Ni bonds and also a U–U bonding interaction.

Magnetic and electronic absorption studies. Variable-temperature magnetic measurements were performed with a superconducting quantum interference device (SQUID) to elucidate further the electronic structures of these multimetallic-bridged clusters (Fig. 4a). The magnetic moment of **3-$U_2Ni_2Cl_2$** at 300 K (6.33 μ_B) was found to be higher than the theoretical magnetic moment for two independent uranium(IV) centres with a $5f^2$ configuration (5.06 μ_B). The magnetic moments of **3-$U_2Ni_2Cl_2$** exhibit a significant temperature dependence, which decrease steadily to 1.39 μ_B at 5 K. The Curie and Curie–Weiss constants for **3-$U_2Ni_2Cl_2$** are 6.95(8) $cm^3\,K\,mol^{-1}$ and −122(9) K, respectively (Supplementary Fig. 11). The negative Curie–Weiss constant and the steadily descending curve of the magnetic moment mainly result from the thermal depopulation of the Stark sublevels and the possible antiferromagnetic coupling[48–50]. The magnetic moments of **4-U_2Ni_2** (4.94 μ_B) and **5-U_2Ni_3** (5.06 μ_B) at 300 K are slightly lower than the theoretical value for two independent uranium(III) centres (5.12 μ_B). With decreasing temperatures, the magnetic moments of **4-U_2Ni_2** and **5-U_2Ni_3** persistently decrease to 1.30 μ_B and 0.82 μ_B at 5 K, respectively (Fig. 4a). In general, the magnetic moment for mononuclear U(III) species at low temperature is usually larger than 1.0 μ_B (ref. [50]). The smaller magnetic moments for **4-U_2Ni_2** (0.92 μ_B per U) and **5-U_2Ni_3** (0.58 μ_B per U) at 5 K are probably due to the U–U interactions and consequent intramolecular antiferromagnetic coupling, which is also in agreement with the negative Curie–Weiss constants (Supplementary Fig. 11). Therefore, the SQUID results are consistent with the theoretical analysis, which proposes the U–U interactions in both **4-U_2Ni_2** and **5-U_2Ni_3**.

The ultraviolet–visible (UV–vis) absorption spectra of **3-$U_2Ni_2Cl_2$**, **4-U_2Ni_2** and **5-U_2Ni_3** were recorded in THF at r.t. (Fig. 4b). All the multimetallic-bridged clusters displayed a broad absorption from 300 to 900 nm, which corresponds with the black crystals observed after recrystallization. The molar absorption coefficients of **4-U_2Ni_2** and **5-U_2Ni_3** were significantly higher than that of **3-$U_2Ni_2Cl_2$** from 300 to 500 nm. In addition, in the near-infrared region, the uranium(III) complexes display two absorption peaks at 1,060 nm (molar absorption coefficient (ε) = ~108 $M^{-1}\,cm^{-1}$) and 1,178 nm (ε = ~98 $M^{-1}\,cm^{-1}$) for **4-U_2Ni_2** (Supplementary Fig. 13) and at 1,125 nm (ε = ~180 $M^{-1}\,cm^{-1}$) and 1,185 nm (ε = ~170 $M^{-1}\,cm^{-1}$) for **5-U_2Ni_3** (Supplementary Fig. 14).

Conclusions

In summary, we report a straightforward strategy to construct a series of transition-metal-bridged bimetallic clusters with multiple uranium–metal bonds, which were supported by a heptadentate N_4P_3 scaffold with three rigid N–P units. The high number of uranium–metal bonds observed in these heterometallic clusters is noteworthy. Both experimental and computational analyses show that the oxidation states of uranium in **4-U_2Ni_2** and **5-U_2Ni_3** are +III and that the electronic configurations of uranium in these species are U(III)-$5f^26d^1$.

This unique N_4P_3 ligand provides an efficient platform for the synthesis of multimetallic clusters with bonding between the *f*-block elements and transition metals. This study offers new opportunities to investigate the possible role of *d*–*f* heterometallic clusters with

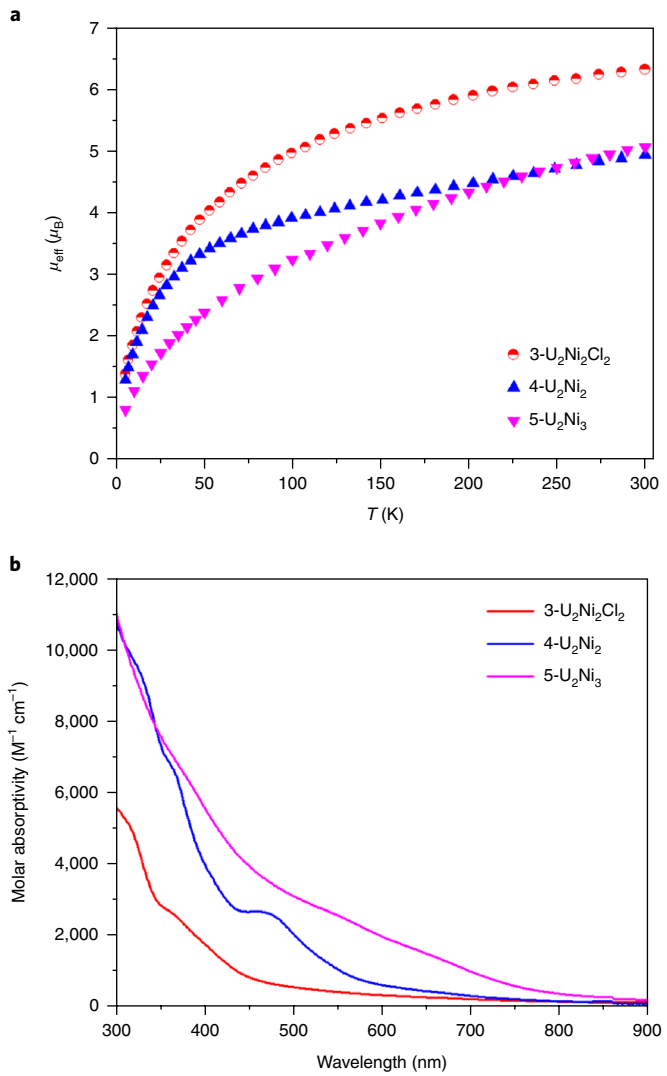

Fig. 4 | Electronic structure studies by SQUID magnetometry and UV–visible absorption spectroscopy. a, Variable-temperature effective magnetic moment data for multimetallic-bridged clusters **3-$U_2Ni_2Cl_2$**, **4-U_2Ni_2** and **5-U_2Ni_3**. The smaller magnetic moments at low temperature for **4-U_2Ni_2** and **5-U_2Ni_3** are probably due to the U-U interactions and consequent intramolecular antiferromagnetic coupling. **b**, UV–visible absorption spectra measured in THF at r.t. for clusters **3-$U_2Ni_2Cl_2$**, **4-U_2Ni_2** and **5-U_2Ni_3**. The molar absorption coefficients of uranium(III) clusters **4-U_2Ni_2** and **5-U_2Ni_3** were significantly higher than that of the uranium(IV) cluster **3-$U_2Ni_2Cl_2$**.

direct metal–metal bonds in small-molecule activation and organic synthesis, and may further promote the development of depleted uranium chemistry. Further studies on the reactivity and catalysis of these *d*–*f* heteromultimetallic clusters are in progress.

Data availability

Crystal data of **1**, **2**, **3-$U_2Ni_2Cl_2$**, **4-U_2Ni_2** and **5-U_2Ni_3** have been deposited at the Cambridge Crystallographic Data Centre (CCDC) under reference numbers CCDC-1842367 (**1**), 1842368 (**2**), 1843093 (**3-$U_2Ni_2Cl_2$**), 1843092 (**4-U_2Ni_2**) and 1842369 (**5-U_2Ni_3**). These data can be obtained free of charge from The Cambridge Crystallographic Data Centre (www.ccdc.cam.ac.uk/data_request/cif). All other data supporting the findings of this study are available within the article and its Supplementary Information, or from the corresponding author upon reasonable request.

Received: 18 May 2018; Accepted: 22 November 2018;
Published online: 28 January 2019

References

1. Adams, R. D. & Cotton, F. A. *Catalysis by Di- and Polynuclear Metal Cluster Complexes* (Wiley-VCH, Weinheim, 1998).
2. Liddle, S. T. *Molecular Metal–Metal Bonds: Compounds, Synthesis, Properties* (Wiley-VCH, Weinheim, 2015).
3. Hill, M. S., Hitchcock, P. B. & Pongtavornpinyo, R. A linear homocatenated compound containing six indium centers. *Science* **311**, 1904–1907 (2006).
4. Butovskii, M. V. et al. Molecules containing rare-earth atoms solely bonded by transition metals. *Nat. Chem.* **2**, 741–744 (2010).
5. Shima, T. et al. Dinitrogen cleavage and hydrogenation by a trinuclear titanium polyhydride complex. *Science* **340**, 1549–1552 (2013).
6. Hu, S., Shima, T. & Hou, Z. Carbon–carbon bond cleavage and rearrangement of benzene by a trinuclear titanium hydride. *Nature* **512**, 413–415 (2014).
7. McWilliams, S. F. & Holland, P. L. Dinitrogen binding and cleavage by multinuclear iron complexes. *Acc. Chem. Res.* **48**, 2059–2065 (2015).
8. MacKay, B. A. & Fryzuk, M. D. Dinitrogen coordination chemistry: on the biomimetic borderlands. *Chem. Rev.* **104**, 385–401 (2004).
9. MacLeod, K. C. & Holland, P. L. Recent developments in the homogeneous reduction of dinitrogen by molybdenum and iron. *Nat. Chem.* **5**, 559–565 (2013).
10. Gagliardi, L. & Roos, B. O. Quantum chemical calculations show that the uranium molecule U_2 has a quintuple bond. *Nature* **433**, 848–851 (2005).
11. Liddle, S. T. & Mills, D. P. Metal–metal bonds in *f*-element chemistry. *Dalton Trans.* 5592–5605 (2009).
12. Chi, C. et al. Preparation and characterization of uranium–iron triple-bonded $UFe(CO)_3^-$ and $OUFe(CO)_3^-$ complexes. *Angew. Chem. Int. Ed.* **56**, 6932–6936 (2017).
13. Fox, A. R., Bart, S. C., Meyer, K. & Cummins, C. C. Towards uranium catalysts. *Nature* **455**, 341–349 (2008).
14. Thomson, R. K. et al. Uranium azide photolysis results in C–H bond activation and provides evidence for a terminal uranium nitride. *Nat. Chem.* **2**, 723–729 (2010).
15. Arnold, P. L. et al. Strongly coupled binuclear uranium–oxo complexes from uranyl oxo rearrangement and reductive silylation. *Nat. Chem.* **4**, 221–227 (2012).
16. Arnold, P. L., Mansell, S. M., Maron, L. & McKay, D. Spontaneous reduction and C–H borylation of arenes mediated by uranium(III) disproportionation. *Nat. Chem.* **4**, 668–674 (2012).
17. Halter, D. P., Heinemann, F. W., Bachmann, J. & Meyer, K. Uranium-mediated electrocatalytic dihydrogen production from water. *Nature* **530**, 317–321 (2016).
18. Zhang, L., Zhang, C., Hou, G., Zi, G. & Walter, M. D. Small-molecule activation mediated by a uranium bipyridyl metallocene. *Organometallics* **36**, 1179–1187 (2017).
19. Edelmann, F. T. Lanthanides and actinides: annual survey of their organometallic chemistry covering the year 2016. *Coord. Chem. Rev.* **338**, 27–140 (2017).
20. Falcone, M., Chatelain, L., Scopelliti, R., Živković, I. & Mazzanti, M. Nitrogen reduction and functionalization by a multimetallic uranium nitride complex. *Nature* **547**, 332–335 (2017).
21. Arnold, P. L. & Turner, Z. R. Carbon oxygenate transformations by actinide compounds and catalysts. *Nat. Rev. Chem.* **1**, 0002 (2017).
22. Halter, D. P., Heinemann, F. W., Maron, L. & Meyer, K. The role of uranium–arene bonding in H_2O reduction catalysis. *Nat. Chem.* **10**, 259–267 (2018).
23. Sternal, R. S. & Marks, T. J. Actinide-to-transition metal bonds. Synthesis, characterization, and properties of metal–metal bonded systems having the tris(cyclopentadienyl) actinide fragment. *Organometallics* **6**, 2621–2623 (1987).
24. Bucaille, A., Le Borgne, T., Ephritikhine, M. & Daran, J. C. Synthesis and X-ray crystal structure of a urana[1]ferrocenophane, the first tris(1,1′-ferrocenylene) metal compound. *Organometallics* **19**, 4912–4914 (2000).
25. Monreal, M. J. & Diaconescu, P. L. A weak interaction between iron and uranium in uranium alkyl complexes supported by ferrocene diamide ligands. *Organometallics* **27**, 1702–1706 (2008).
26. Gardner, B. M., McMaster, J., Lewis, W. & Liddle, S. T. Synthesis and structure of $[\{N(CH_2CH_2NSiMe_3)_3\}URe(\eta^5\text{-}C_5H_5)_2]$: a heterobimetallic complex with an unsupported uranium–rhenium bond. *Chem. Commun.* 2851–2853 (2009).
27. Patel, D. et al. A formal high oxidation state inverse-sandwich diuranium complex: a new route to *f*-block-metal bonds. *Angew. Chem. Int. Ed.* **50**, 10388–10392 (2011).
28. Fortier, S., Walensky, J. R., Wu, G. & Hayton, T. W. High-valent uranium alkyls: evidence for the formation of $U^{VI}(CH_2SiMe_3)_6$. *J. Am. Chem. Soc.* **133**, 11732–11743 (2011).
29. Gardner, B. M. et al. The nature of unsupported uranium–ruthenium bonds: a combined experimental and theoretical study. *Chem. Eur. J.* **17**, 11266–11273 (2011).

30. Gardner, B. M. et al. An unsupported uranium–rhenium complex prepared by alkane elimination. *Chem. Eur. J.* **17**, 6909–6912 (2011).
31. Patel, D. et al. Structural and theoretical insights into the perturbation of uranium–rhenium bonds by dative Lewis base ancillary ligands. *Chem. Commun.* **47**, 295–297 (2011).
32. Napoline, J. W. et al. Tris(phosphinoamide)-supported uranium–cobalt heterobimetallic complexes featuring Co→U dative interactions. *Inorg. Chem.* **52**, 12170–12177 (2013).
33. Ward, A. L., Lukens, W. W., Lu, C. C. & Arnold, J. Photochemical route to actinide–transition metal bonds: synthesis, characterization and reactivity of a series of thorium and uranium heterobimetallic complexes. *J. Am. Chem. Soc.* **136**, 3647–3654 (2014).
34. Senchyk, G. A. et al. Hybrid uranyl–vanadium nano-wheels. *Chem. Commun.* **51**, 10134–10137 (2015).
35. Hlina, J. A., Pankhurst, J. R., Kaltsoyannis, N. & Arnold, P. L. Metal–metal bonding in uranium–group 10 complexes. *J. Am. Chem. Soc.* **138**, 3333–3345 (2016).
36. Hlina, J. A., Wells, J. A., Pankhurst, J. R., Love, J. B. & Arnold, P. L. Uranium–rhodium bonding in heterometallic complexes. *Dalton. Trans.* **46**, 5540–5545 (2017).
37. Fortier, S. et al. An N-tethered uranium (III) arene complex and the synthesis of an unsupported U–Fe bond. *Organometallics* **36**, 4591–4599 (2017).
38. Lu, E., Wooles, A., Gregson, M., Cobb, P. & Liddle, S. T. A very short uranium(IV)–rhodium(I) bond with net double-dative bonding character. *Angew. Chem. Int. Ed.* **57**, 6587–6591 (2018).
39. Greenwood, B. P., Rowe, G. T., Chen, C. H., Foxman, B. M. & Thomas, C. M. Metal–metal multiple bonds in early/late heterobimetallics support unusual trigonal monopyramidal geometries at both Zr and Co. *J. Am. Chem. Soc.* **132**, 44–45 (2010).
40. Culcu, G. et al. Heterobimetallic complexes comprised of Nb and Fe: isolation of a coordinatively unsaturated Nb^{III}/Fe^{0} bimetallic complex featuring a Nb≡Fe triple bond. *J. Am. Chem. Soc.* **139**, 9627–9636 (2017).
41. Rudd, P. A. et al. Metal–alane adducts with zero-valent nickel, cobalt, and iron. *J. Am. Chem. Soc.* **133**, 20724–20727 (2011).
42. Eisenhart, R. J., Clouston, L. J. & Lu, C. C. Configuring bonds between first-row transition metals. *Acc. Chem. Res.* **48**, 2885–2894 (2015).
43. Sgro, M. J. & Stephan, D. W. Frustrated Lewis pair inspired carbon dioxide reduction by a ruthenium tris(aminophosphine) complex. *Angew. Chem. Int. Ed.* **51**, 11343–11345 (2012).
44. Gardner, B. M. & Liddle, S. T. Uranium triamidoamine chemistry. *Chem. Commun.* **51**, 10589–10607 (2015).
45. Pyykkö, P. & Atsumi, M. Molecular single-bond covalent radii for elements 1–118. *Chem. Eur. J.* **15**, 186–197 (2009).
46. Ritchey, J. M. et al. An organothorium–nickel phosphido complex with a short Th–Ni distance. The structure of $Th(\eta^5\text{-}C_5Me_5)_2(\mu\text{-}PPh_2)_2Ni(CO)_2$. *J. Am. Chem. Soc.* **107**, 501–503 (1985).
47. Hay, P. J., Ryan, R. R., Salazar, K. V., Wrobleski, D. A. & Sattelberger, A. P. Synthesis and X-ray structure of $(C_5Me_5)_2Th(\mu\text{-}PPh_2)_2Pt(PMe_3)$: a complex with a thorium–platinum bond. *J. Am. Chem. Soc.* **108**, 313–315 (1986).
48. Rinehart, J. D., Harris, T. D., Kozimor, S. A., Bartlett, B. M. & Long, J. R. Magnetic exchange coupling in actinide-containing molecules. *Inorg. Chem.* **48**, 3382–3395 (2009).
49. Mills, D. P. et al. A delocalized arene-bridged diuranium single-molecule magnet. *Nat. Chem.* **3**, 454–460 (2011).
50. Kindra, D. R. & Evans, W. J. Magnetic susceptibility of uranium complexes. *Chem. Rev.* **114**, 8865–8882 (2014).

Acknowledgements

This research was supported by the National Natural Science Foundation of China (grant no. 21772088), the Natural Science Foundation of Jiangsu Province (grant no. BK20170635), the Fundamental Research Funds for the Central Universities, the program of Jiangsu Specially-Appointed Professor and the Young Elite Scientist Sponsorship Program of the China Association of Science and Technology. The authors thank Y. Song (Nanjing University) and S. Jiang (Peking University) for useful discussion.

Author contributions

C.Z. conceived this project. G.F. performed the synthesis experiments. M.Z. solved all of the X-ray structures. D.S. performed the SQUID experiments. C.Z. and G.F. analysed the experimental data. L.M. conducted the theoretical computations and analysed the results. C.Z. and L.M. drafted the paper with support from G.F., X.W. and S.W. All the authors discussed the results and contributed to the preparation of the final manuscript.

Competing interests

The authors declare no competing interests.

Additional information

Supplementary information is available for this paper at https://doi.org/10.1038/s41557-018-0195-4.

Reprints and permissions information is available at www.nature.com/reprints.

Correspondence and requests for materials should be addressed to L.M. or C.Z.

Publisher's note: Springer Nature remains neutral with regard to jurisdictional claims in published maps and institutional affiliations.